Journal of Solid State Chemistry 183 (2010) 2475–2482

Contents lists available at ScienceDirect

Journal of Solid State Chemistry

journal homepage: www.elsevier.com/locate/jssc

Synthesis, structure, solid-state thermolysis, and thermodynamic properties of new heterometallic complex $Li_2Co_2(Piv)_6(NEt_3)_2$

Zn.V. Dobrohotova [a], A.A. Sidorov [a], M.A. Kiskin [a,*], G.G. Aleksandrov [a], K.S. Gavrichev [a], A.V. Tyurin [a], A.L. Emelina [b], M.A. Bykov [b], A.S. Bogomyakov [c], I.P. Malkerova [a], A.S. Alihanian [a], V.M. Novotortsev [a], I.L. Eremenko [a]

[a] N.S. Kurnakov Institute of General and Inorganic Chemistry, Russian Academy of Sciences, Leninsky Prosp. 31, 119991 Moscow, GSP-1, Russian Federation
[b] Department of Chemistry, M.V. Lomonosov Moscow State University, 1 Leninskie Gory, 119992 Moscow, Russian Federation
[c] International Tomography Centre, Siberian Branch of the Russian Academy of Sciences, Institutskaya Str. 3a, 630090 Novosibirsk, Russian Federation

ARTICLE INFO

Article history:
Received 18 June 2010
Accepted 6 August 2010
Available online 12 August 2010

Keywords:
Cobalt
Lithium
Heterometallic complex
X-ray analysis
Thermal decomposition
Heat capacity
Thermodynamics

ABSTRACT

The reaction of lithium pivalate, polymeric cobalt pivalate $[Co(Piv)_2]_n$, and triethylamine in THF at 60 °C afforded the new heterometallic antiferromagnetic complex $Li_2Co_2(Piv)_6(NEt_3)_2$ (**2**). The molecular and crystal structure of complex **2** was established and its magnetic behavior was studied. The vaporization and solid-state thermolysis of **2** were investigated. The thermodynamic characteristics of complex **2** were determined. The results of the present study show that complex **2** can be used as a potential molecular precursor for the synthesis of thin films of lithium cobaltate $LiCoO_2$.

1. Introduction

The possibility of application of polynuclear coordination compounds as molecular precursors for the directed synthesis of various inorganic materials of desired composition and with desired structure has been actively investigated in the last three decades [1–9]. As for complex oxides, this aim can be achieved by specifying the composition of the target oxides and, probably, their properties already when preparing the corresponding coordination compounds as their molecular precursors. The target oxides can be formed from the precursors after the removal of the "organic moiety" under relatively mild conditions (below 500 °C). This "prognostic" methodology has attracted great attention of researchers. Thus, the thermal behavior of three coordination compounds $[Fe_2Ni(C_4H_4O_5)_{2.5}(OH)_2]\cdot NO_3\cdot 5H_2O$, $[Fe_2Ni(C_4H_8O_3N_2)_4]\cdot 8NO_3\cdot 24H_2O$, and $(NH_4)[Fe_2Ni(C_4H_4O_5)_3(OH)_3]\cdot 3H_2O$, which are formally potential precursors of nickel ferrite, was investigated [10]. In the studies [11,12], heterometal copper and zinc complexes with ethylenediamine and the heterometal Cu^{II}/Mn^{II} oxalate complex with ethylenediamine were considered as the starting compounds for the synthesis of inorganic ceramic materials, which can be used as electrocatalysts in the oxygen reduction. Recently, it has been demonstrated that mixed-metal Cu–Co and Ni–Cu oxide thin films can be prepared starting from molecular heterometal cubane-type precursors [13]. It was shown [14] that the decomposition of $M^1[M^2(C_2O_4)_2]\cdot xH_2O$ ($x=5$ for $M^1=Co$; $x=4$ for $M^1=Cd$; $M^2=Ni$) in air afforded oxides $MNiO_x$ ($x=3$ for $M=Co$; $x=2$ for $M=Cd$) at 325 and 360 °C, respectively. It is important that the molecular precursors be available and the metal ratio be unchanged during thermolysis. Examples are the complexes $[Li(H_2O)M(N_2H_3CO_2)_3]\cdot 0.5H_2O$ ($M=Co$ or Ni), whose thermolysis affords materials of composition $LiMO_2$ [15]. However, it should be noted that the starting heterometallic precursors were synthesized in very low yield, which is a serious obstacle to further progress in this field. A different situation occurs when the heterometallic coordination polymer $[Li_2Co_2(Piv)_6(\mu\text{-}L)_2]_n$ (**1**, L=2-amino-5-methylpyridine) is used as the starting precursor. This compound can be prepared in a yield higher than 80% [16]. The thermal decomposition of this polymer (400–500 °C) affords $LiCoO_2$ in quantitative yield. It should be emphasized that it is rational to optimize the conditions for the thermal synthesis of materials based on the data on the thermodynamic properties of the starting compounds [17]. When using the metal-organic deposition (MOD) method (deposition by thermal decomposition of organometallic compounds from solution), which is a special case of the sol–gel method, it is necessary to know the structural characteristics of the precursor and its

* Corresponding author. Fax: +7 495 952 1279.
E-mail address: mkiskin@igic.ras.ru (M.A. Kiskin).

0022-4596/$ - see front matter © 2010 Elsevier Inc. All rights reserved.
doi:10.1016/j.jssc.2010.08.007

thermal stability in the condensed phase. The synthesis of complex oxide films by the metal-organic chemical vapor deposition (MOCVD) technique involves the transfer of the starting compounds into the gas phase as a key step, and it is necessary to know the vapor pressure of the complexes to optimize the evaporation process.

The aim of the present study was to synthesize the new precursor lithium cobaltate and to perform comprehensive physicochemical investigation.

2. Experimental

2.1. Synthesis

New complex **2** was synthesized with the use of freshly distilled THF. The starting cobalt pivalate $[Co(Piv)_2]_n$ was prepared according to a known procedure [18]. In the synthesis of complex **2**, commercial triethylamine (Fluka) was used.

2.1.1. Synthesis of $Li_2Co_2(Piv)_6(NEt_3)_2$ (**2**)

Tetrahydrofuran (30 mL) was added to a mixture of the complex $[Co(Piv)_2]_n$ (0.4 g, 1.54 mmol), triethylamine (0.16 g, 1.54 mmol), and LiPiv (0.17 g, 1.54 mmol). The reaction mixture was heated at 60 °C for 30 min. Then the solution was filtered, concentrated to 10 mL, and cooled to room temperature. Blue crystals that precipitated after 24 h were separated from the solution by decantation, washed with cold THF, and dried under argon. The yield of compound **2** was 0.69 g (95%). Found (%): C, 53.60; H, 8.81; N, 2.85. Calculated for $C_{48}Co_2H_{68}Li_2N_2O_{12}$ (%): C, 53.62; H, 9.00; N, 2.98.

2.2. Methods

The elemental analysis of complex **2** was carried out on an Euro Vector Element Analyser (Model EA 3000). The magnetochemical measurements were performed on a MPMS*XL* SQUID magnetometer (Quantum Design) in the 2–300 K temperature range at a magnetic field strength $H=5$ kOe. The molar magnetic susceptibility χ was calculated taking into account the atomic diamagnetism according to Pascal's additivity rules. In the paramagnetic region, the effective magnetic moment was calculated by the equation $\mu_{eff}=[(3k/N_A\beta^2)\chi T]^{1/2}\approx(8\chi T)^{1/2}$, where k is the Boltzmann constant, N_A is Avogadro's number, and β is the Bohr magneton.

2.3. X-ray data collection

The X-ray diffraction study of complex **2** was carried out on Bruker SMART APEX II diffractometer equipped with a CCD camera and a graphite monochromated Mo$K\alpha$ radiation source ($\lambda=0.71073$ Å) [19]. The X-ray data were collected in the range $1.05<\theta<28.00$ ($-15\le h\le 15$, $-16\le k\le 16$, $-26\le l\le 26$) using the ω scan mode. The structure was solved by direct methods [20] and refined by full-matrix least-squares on F^2 [21] with anisotropic thermal parameters for all non-hydrogen atoms. The hydrogen atoms of the carbon-containing ligands were positioned geometrically and refined using a riding model. The positions of all methyl carbon atoms in the disordered CMe_3 fragments were located in difference Fourier maps and refined with occupancy of 0.533(6) and 0.467(6) for *tert*-butyl group at the atom C(2), 0.647(6) and 0.353(6) at the atom C(27), and 0.615(6) and 0.385(6) at the atom C(37). The crystallographic parameters for complex **2** at $T=173$ K are as follows: $C_{42}H_{84}Co_2Li_2N_2O_{12}$, $fw=940.85$, blue, prismatic, crystal size $0.25\times0.25\times0.15$, the triclinic system, space group $P-1$, $a=11.9667(5)$, $b=12.7779(6)$, $c=20.4113(12)$ Å, $\alpha=103.4220(10)^\circ$, $\beta=94.1020(10)^\circ$, $\gamma=117.8040(10)^\circ$, $V=2626.0(2)$ Å^3, $Z=2$, $\rho_{calc}=1.190$ g cm^{-3}, $\mu=6.85$ cm^{-1}, 26 814 measured reflections, 12 509 reflections with $I>2.0\sigma(I)$, $R_{int}=0.0202$, $GooF=1.057$, $R_1(I>2\sigma(I))=0.0664$, w$R_2(I>2\sigma(I))=0.1828$, R_1(all data)$=0.0794$, wR_2(all data)$=0.1924$, $T_{min/max}=0.8475/0.9043$.

2.4. Thermal decomposition

The thermal decomposition of compound **2** was studied by differential scanning calorimetry (DSC) and thermogravimetry (TGA). The thermogravimetric measurements were performed in an artificial air flow (20 ml/min) and in an argon flow (20 ml/min) on a *NETZSCH TG 209 F1* instrument in alundum crucibles at a heating rate of 10 °C/min. The composition of the gas phase below 250 °C was studied by thermogravimetry-mass spectrometry on a QMS 403C Aolos mass-spectrometric unit. The ionizing electron energy was 70 eV; the largest determined mass number (the mass-to-charge ratio) was 300 amu. The weight of the samples for thermogravimetric experiments was 0.5–3 mg. The differential scanning calorimetry in a dry artificial air flow (O_2, 20.8%; CH_4, <0.0001%) and in an argon flow (Ar, >99.998%; O_2, 0.0002%; N_2, <0.001%; aqueous vapor, <0.0003%; CH_4, <0.0001%) was carried out on a *NETZSCH DSC 204 F1* calorimeter in aluminum cells at a heating rate of 10 °C/min. The weight of the samples was 4–10 mg. Each experiment was repeated at least three times. The temperature scales and the calorimeter were calibrated against the phase transition temperatures of standard compounds (C_6H_{12}, Hg, KNO_3, In, Sn, Bi, and CsCl; 99.99% purity; ISO/CD 11357-1).

2.5. Mass spectrometry

The vaporization of the complex $Li_2Co_2(Piv)_6(NEt_3)_2$ (**2**) was studied by the Knudsen effusion method with mass-spectrometric analysis of the gas-phase composition in the 353–530 K (80–257 °C) temperature range on a MC 1301 instrument. The experiments were carried out in a standard molybdenum cell with a ratio of the effusion orifice to the vaporization surface of ≈ 600. The temperature was measured by a Pt–Pt(Rh) thermal couple with an accuracy of $\pm 1^\circ$. The mass spectrum of the gas phase over the compound is presented in Table S1.

2.6. Heat capacity

The heat capacity was measured by adiabatic calorimetry on a BKT-3 low-temperature adiabatic calorimeter designed and built in the Termis joint-stock company. The measurements were carried out in an automatic mode using a system consisting of a PC and an analog-control and data-collection unit. Samples were placed in a titanium thin-walled cylindrical container with an inner volume of 1 cm^3. The container was sealed in a special chamber under a helium atmosphere at a pressure of about 0.3 bar. The sample weight was 0.43007 g. The temperature of the calorimeter was measured by a rhodium iron resistance thermometer. The sensitivity of the thermometric system was 1×10^{-3} K; the sensitivity of the analog digital converter was 0.1 μV. The energy equivalent of the calorimeter was determined by measuring the heat capacity of an empty ampoule filled with gaseous helium under a pressure of 8.5 kPa. The measurement procedure was tested by comparison measurements of the heat capacity of reference benzoic acid (K-2 grade). The error of the measurement of the heat capacity at helium temperatures was ± 2%, which decreased to ± 0.4% as the temperature increased to 40 K, and was equal to ± 0.2% in the $40-350$ K temperature range. The apparatus and the measurement procedure were

described in detail in [22]. The results of measurements are given in Table S2.

The experimental data obtained by adiabatic calorimetry were smoothed using Eq. (1) [23,24]:

$$C_p^{\circ}(T) = a_0 T C_V^2 + n\left[\frac{1}{3}\sum_{j=1}^{3} a_j D_j \frac{\theta_j}{T} + a_4 E\frac{\theta_E}{T} + a_5 K\left(\frac{\theta_L}{T}, \frac{\theta_U}{T}\right)\right] \quad (1)$$

where n is the number of atoms in the molecule of the complex, D and E are the Debye and Einstein functions, respectively, K is the Kieffer (K) function [25], θ_1, θ_2, θ_3, θ_E, θ_L, and θ_U are the characteristic temperatures, and a_0, a_1, a_2, a_3, a_4, and a_5 are the linear coefficients. The first member of the equation $a_0 T C_V^2$ corresponds to the contribution of the work of lattice expansion. The parameters $a_0 - a_5$ and $\theta_1 - \theta_U$ were determined by the nonlinear least-squares method. The calculation procedure was described in detail in [26]. Eq. (1) was used also for the calculations of the entropy, the change in the enthalpy, and the reduced Gibbs energy of the complexes.

2.7. Kinetic analysis

The kinetic analysis of the first step of the thermolysis of complex **2** was based on non-isothermal DSC curves obtained at four constant heating rates (5, 10, 15, and 20 deg./min). The calculations were carried out with the use of the NETZSCH Thermokinetics 3 program.

The reaction rate was described by the equation

$$\frac{dx}{dt} = f(x) k_0 \exp\left(-\frac{E}{RT}\right) \quad (2)$$

where dx/dt is the reaction rate, $f(x)$ is the function describing the relationship between the reaction rate and the degree of conversion x (kinetic equation), k_0 and E are the temperature-independent reaction parameters, such as the frequency factor and the activation energy, respectively, R is the universal gas constant, and T is the temperature in terms of the formal kinetics of homogeneous reactions. This approach is often used in the analysis of TMA data [27,28].

The formal model of the reaction mechanism was determined by non-*a-priori* Friedman [29], Ozawa–Flynn–Wall [30,31], and model-fitting [32] methods.

A substantial advantage of the non-*a-priori* methods is that the results of calculations are independent of the type of kinetic equation $f(x)$. The parameters of the kinetic model determined by isoconversional methods' parameters are correct and are well consistent with both each other and with the results of other physicochemical methods [33–35].

In the model-fitting methods [28,32,36], the number and the order of the reaction steps and the type of kinetic equations are a priori specified. These initial conditions are generally chosen based on non-*a-priori* methods. The parameters of the kinetic equations are evaluated by the approximation of experimental points. The main advantages of these methods over non-*a-priori* methods are that, first, the type and parameters of the equation $f(x)$ can be determined and, second, these methods can be used for the analysis of complex reactions involving competitive and independent steps. The reliability of the results can be estimated based on Fisher's statistical test (the validity of the model, the significance of the additional reaction steps), as well as based on the agreement between the results obtained by non-*a-priori* and model-fitting methods.

2.8. Electron microscopy

Photomicrographs of $LiCoO_2$ samples were taken on a JEOL JSM 6490 LV scanning electron microscope equipped with an INCA system for elemental analysis. Conducting thin-film samples were placed in a chamber and the chamber was evacuated to the residual pressure of 10^{-6} mm Hg. The primary electron beam energy was 25 keV; the focus distance was 10 mm.

3. Results and discussion

Recently, we have shown that the heterometallic polymer $[Li_2Co_2(Piv)_6(\mu\text{-}L)_2]_n$ (**1**, L=2-amino-5-methylpyridine) is a promising molecular precursor for the synthesis of thin films of the cathode material $LiCoO_2$. This polymer is formed in high yield (81%) in the reaction of polymeric cobalt pivalate $[Co(Piv)_2]_n$, lithium pivalate LiPiv (Co:Li=1:1), and 2-amino-5-methylpyridine in a THF-MeCN medium [16]. Although the thermolysis of **1** affords lithium cobaltate in quantitative yield, aminomethylpyridine is eliminated at relatively high temperature (260 °C), which in principle does not exclude the possibility of catalytic decomposition of the ligand giving rise to amorphous carbon materials. These effects make the precise determination of the thermodynamic parameters difficult. This, in turn, causes problems in the development of an efficient temperature program for decomposition. To resolve this problem, in the present study we used more convenient and easily removed triethylamine instead of aminomethylpyridine.

3.1. Synthesis, structure, and magnetic properties of the heterometallic complex $Li_2Co_2(Piv)_6(NEt_3)_2$

Heterometallic complex **2** was synthesized by the direct reaction of lithium pivalate, polymeric cobalt pivalate $[Co(Piv)_2]_n$, and triethylamine in THF at 60 °C and was isolated as blue crystals. According to the X-ray diffraction data, there are two independent chemically identical molecules of complex **2** per asymmetric unit (Fig. 1). The metal core of **2** is a zigzag chain CoLiLiCo. All atoms of the chain lie in one plane. Molecule **2** consists of two identical $LiCo(Piv)_3(NEt_3)$ fragments, in which each cobalt atom is bound to the nitrogen atom of the triethylamine ligand (selected geometric characteristics of complex **2** are given in Table 1). The cobalt and lithium atoms are linked by three pivalate bridges. All bridging anions are differently bound to the metal atoms. Two of the ligands act as a bidentate bridges, and the third ligand serves as a tridenatate bridge, in which one oxygen atom is coordinated to the cobalt atom and another oxygen atom is coordinated to two lithium atoms. This provides the binding of two Li–Co fragments through two Li–O bonds. The center of symmetry of molecule **2** lies at the intersection of the diagonals of the almost square O_2Li_2 fragment.

Each cobalt atom is in a strongly distorted tetrahedral environment formed by three oxygen atoms of the bridging pivalate anions and the nitrogen atom of the neutral N-donor ligand. The N–Co–O angles are substantially smaller than the O–Co–O angles, which is indicative of a strong distortion of the O_3N tetrahedron almost to a trigonal pyramid. Taking into account this contact, the latter group can formally be considered as a chelate bridging ligand. The closure of one of the bridging groups to a chelate ring results in the relatively rigid fixation of the adjacent Co and Li atoms. In addition, the binding of one of the bridging anions to the second lithium atom places additional restrictions on its conformational flexibility, resulting in the unexpectedly high geometric rigidity of the zigzag chain CoLiLiCo.

The magnetic measurements showed that the effective magnetic moment of compound **2** at room temperature is 6.40 μ_B (per molecule) (Fig. 2a) or 4.53 μ_B (per cobalt atom), which is close to the experimental values for the high-spin Co^{II} atoms (S=3/2) taking into account the spin–orbital interaction (4.4–5.2 μ_B) [37]. The lowering of the temperature leads to a

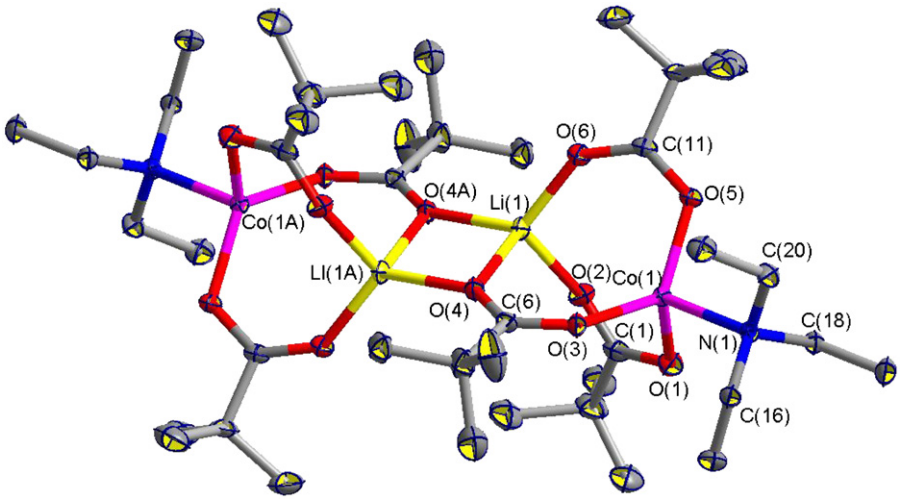

Fig. 1. Molecular structure of complex **2** (one independent molecule is shown; the hydrogen atoms are omitted; 30% thermal probability ellipsoids).

Table 1
Selected geometric characteristics of complex **2** (for two independent molecules).

Parameter	Value
Li–Li–Co, deg.	121.0(3), 123.2(3)
Li–Co–N, deg.	169.32(13),171.42(14)
Li–O–Li, deg.	80.8(2), 82.2(3)
O–C–O, deg.	124.1(3)–128.3(3)
Co…Li (Å)	3.250(6), 3.330(8)
Li…Li (Å)	2.644(11), 2.696(11)
Co–N (Å)	2.229(3), 2.281(3)
Co–O (Å)	1.864(3)–2.011(2)
Li–O (Å)	1.715(6)–2.103(7)
C–O (Å)	1.181(5)–1.363(5)

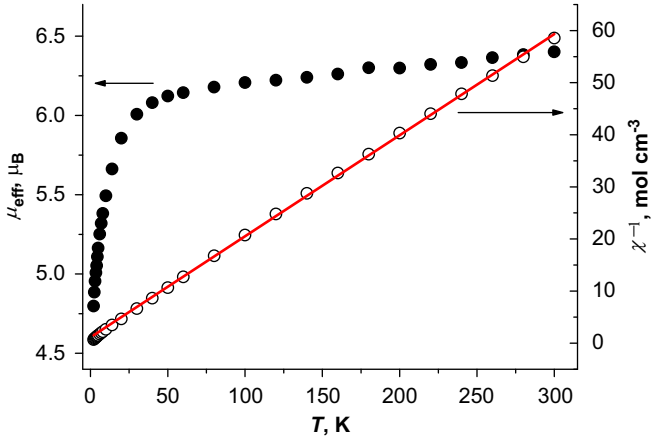

Fig. 2. Magnetic properties of complex **1** (the temperature dependence of the magnetic moment (●); the curve $1/\chi$ (○) and the calculated data represented by a line).

decrease in μ_{eff} down to 4.80 μ_B at 2 K, which is typical of systems with high-spin cobalt(II) atoms and can be assigned to the spin–orbital effect.

In the 15–300 K temperature range, the dependence $\chi^{-1}(T)$ for complex **2** follows the Curie–Weiss law ($\chi=C/(T-\theta)$) with $C=5.155$ cm^3 K/mol (2.58 cm^3 K/mol per Co^{II} ion) and $\theta/k=-5.8$ K (Fig. 2b). The value $C=2.58$ is higher than the theoretical value for the pure-spin state ($C=1.875$ for $S=3/2$ and $g=2$) due to the orbital contribution to the magnetic susceptibility typical of Co^{II} ions and the g-factor values larger than 2.

3.2. Thermal decomposition, mass spectrometry, and heat capacity

The TGA measurements showed that the decomposition of complex **2** during heating both in air and under an inert atmosphere occurs without the formation of stable intermediates (Fig. 3a). The experimental DSC curves measured in air and under an inert atmosphere also have common features (Fig. 3b). The DSC curves show two steps. The first step is endothermic, whereas the second step is exothermic.

The first decomposition step ($T=140$–200 °C) leads to the elimination of triethylamine. This is confirmed by data for the gas phase obtained by thermogravimetry-mass-spectrometry. These experiments showed that only triethylamine molecules are present among gaseous decomposition products with $Z<300$ amu.

The endothermic peaks in the DSC curves (Fig. 3*b*) ($T_{onset}=149$ °C (in air) and $T_{onset}=140$ °C (under argon), $Q=160.7\pm5.2$ (in air) and $Q=158.3\pm3.5$ (under argon) kJ/mol for complex **2**) correspond to the weight loss of $19.5\pm1.5\%$ and $19.0\pm1.5\%$ in air and under argon, respectively. The content of triethylamine in complex **2** calculated from the empirical molecular formula is 21.49%. We can say with some certainty that the total thermal effect of the first step of solid-state thermal decomposition of the complex with triethylamine corresponds to a change in the enthalpy of the reaction:

$$Li_2Co_2(Piv)_6(NEt_3)_2(sol)=Li_2Co_2(Piv)_6(sol)+2NEt_3(gas)$$

In the 200–350 °C temperature range, complex **2** undergoes further destructive decomposition with relatively high energy release, which is apparently attributed to the formation of new structures of the solid decomposition product and, in air, to the oxidation of intermediate decomposition products by oxygen.

According to the X-ray powder diffraction data, the solid decomposition product of complex **2** under an inert atmosphere at temperature below 500 °C is a heterogeneous mixture of cobalt oxide CoO and lithium oxide Li_2O (Table S3). The weight of the solid residue was $18.1\pm1.5\%$ of the starting weighed sample, which agrees within experimental error with the value (19.15%) calculated from the empirical molecular formula on the assumption that the decomposition affords a mixture of the phases Li_2O and CoO. According to the X-ray powder diffraction data, the solid

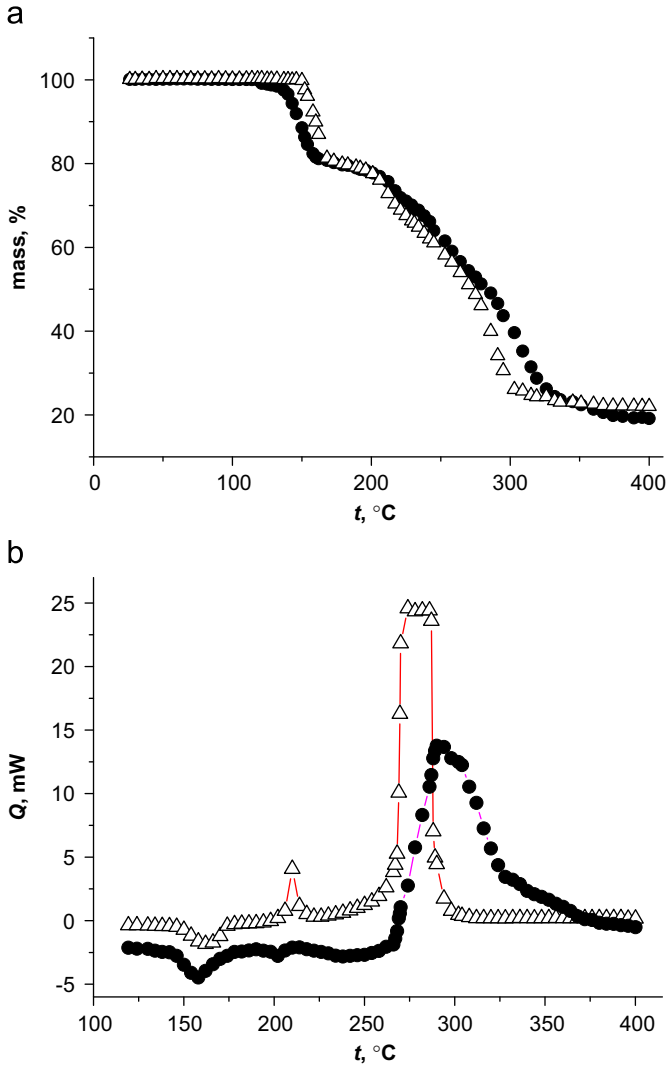

Fig. 3. Temperature dependence of the weight loss (a) and the heat flux (b) during heating of complex **2** (△, in air; ●, under an inert atmosphere).

product obtained upon decomposition in air in the TGA and DSC experiments at temperatures below 500 °C without the subsequent storage under temperature-controlled conditions is a heterogeneous mixture of cobalt oxide Co_3O_4, lithium oxide Li_2O, and lithium cobaltate $LiCoO_2$ (Table S3). The subsequent storage of the thermolysis product under temperature-controlled conditions at 500 °C for 30–90 min led to the complete disappearance of reflections corresponding to simple oxides in the X-ray diffraction patterns. The weight of the solid residue obtained upon thermolysis in air was 20.0 ± 1.5% of the starting weighed sample, which agrees within experimental error with the value (20.85%) calculated from the empirical molecular formula on the assumption that the decomposition affords $LiCoO_2$.

The study of the vaporization process showed (Table S1) that a saturated vapor of the complex contained NEt_3 and $Li_2Co_2(Piv)_6$ molecules.

To determine the quantitative composition of the vapor and the character of vaporization of $Li_2Co_2(Piv)_6(NEt_3)_2$, we measured the isotherm of complete vaporization of the known weighed sample (Fig. 4). In the initial step of vaporization at temperature below 415 K, the recorded ionic currents until the complete decay indicate that the vapor contains exclusively triethylamine molecules. After a further increase in temperature, the original mass spectrum was restored. The ionic currents from $[LiCo_3(Piv)_5+CH_2CCOO]^+$ and $[LiCo_3(Piv)_6]^+$ remained constant during a certain period of time and then disappeared.

The intensities of all other ionic currents remained constant throughout the vaporization process. After completion of the experiment, a nonvolatile residue was absent in an effusion cell. The above-described results suggest that all the detected ions correspond to the mass spectrum of a saturated vapor of the intermediate $Li_2Co_2(Piv)_6$ (sol) consisting of the dimeric molecules $Li_2Co_2(Piv)_6$ and reflect the congruent character of vaporization of the latter.

Based on the analysis of the mass-spectrometric results and the data obtained using complete isothermal vaporization, the vaporization of $Li_2Co_2(Piv)_6(NEt_3)_2$ can be represented by the following reactions:

$$Li_2Co_2(Piv)_6(NEt_3)_2 = Li_2Co_2(Piv)_6(sol) + 2NEt_3(gas)\ (T < 415\ K) \quad (3)$$

$$Li_2Co_2(Piv)_6(sol) = Li_2Co_2(Piv)_6(gas) \quad (4)$$

Data on the complete isothermal vaporization allowed us to calculate the absolute values of the partial pressures of the components in the saturated vapor over $Li_2Co_2(Piv)_6(NEt_3)_2$ by the Hertz–Knudsen equation. In the calculations, we used atomic ionization cross-sections [38] and the additivity rule [39]. At $T=360$ K, $P_{(NEt3)}=3.1\times10^{-1}$ Pa. The partial pressure (P, $T=504$ K) of $Li_2Co_2(Piv)_6$ molecules is 2.3×10^{-1} Pa. To determine the enthalpy of sublimation of the intermediate $Li_2Co_2(Piv)_6$, we investigated the temperature dependences of the ionic current intensity: I $[LiCo_2(Piv)_4]^+$, I $[Li_2(Piv)]^+$, I $[Li_2Co(Piv)_3]^+$, I $[LiCo(Piv)_2]^+$, I $[Li_2Co_2(Piv)_5]^+$ in the 465–530 K temperature range. The enthalpies of sublimation were calculated according to the Clausius–Clapeyron equation by the least-squares method. The average value of $\triangle_sH^0[Li_2Co_2(Piv)_6, sol, T]$ obtained from ten independent experiments is 175.6 ± 7.2 kJ/mol. The above determination error is the rms error of the arithmetic mean for a series of measurements. The enthalpy of reaction *2* was evaluated analogously based on the second law of thermodynamics. We obtained $\triangle_sH^0[1, T]=151$ kJ/mol with increase in temperature in the 368–415 K range only for one series of measurements because of the unstable behavior of ionic currents corresponding to the ionization of triethylamine molecules. It should be noted that the results of DSC measurements for process *2* under an inert atmosphere and in air do not contradict the above data. By combining the data on the vapor pressure and the enthalpies of sublimation, we get an analytical expression for the temperature dependence of the vapor pressure over the intermediate

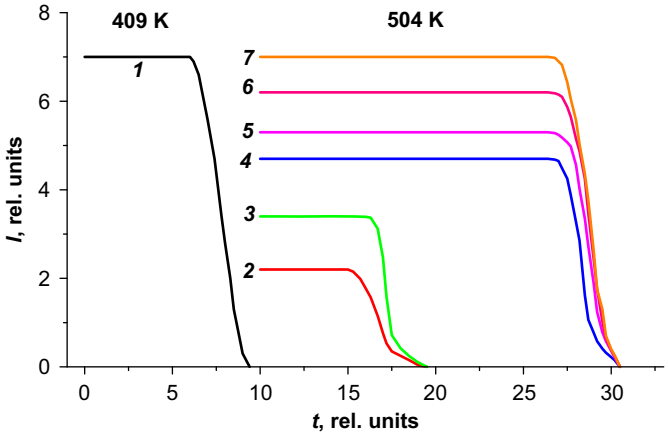

Fig. 4. Isotherm of complete vaporization of compound **2**: *1* – $C_5H_{12}N^+$, *2* – $LiCo_3(Piv)_5+CH_2CCOO]^+$, *3* – $[LiCo_3(Piv)_6]^+$, *4* – $[Li_2Co(Piv)_3]^+$, *5* – $[LiCo_2(Piv)_4]^+$, *6* – $[Li_2Co_2(Piv)_5]^+$, *7* – $[LiCo(Piv)_2]^+$.

Table 2
Thermodynamic functions of compound **2**.

T, K	J/(K mol)			J/mol
	$C_p^0(T)$	$S^0(T)$	$\Phi^0(T)$	$H^0(T)-H^0(0)$
10	34.7440	11.62	2.676	89.43
15	73.9724	33.01	9.021	359.8
20	115.978	59.99	18.30	833.8
25	159.427	90.52	29.64	1522
30	202.984	123.4	42.51	2428
35	245.316	157.9	56.52	3550
40	285.089	193.3	71.40	4877
45	321.428	229.0	86.93	6395
50	355.557	264.7	102.9	8088
60	424.433	335.5	135.8	11980
70	496.3	406.4	169.4	16590
80	554.1	476.7	203.4	21860
90	603.3	544.8	237.6	27650
100	652.1	610.9	271.6	33920
110	699.5	675.2	305.4	40680
120	746.0	738.1	338.8	47910
130	791.7	799.6	371.9	55600
140	836.1	859.9	404.6	63740
150	879.2	919.1	437.0	72320
160	920.7	977.2	468.9	81320
170	960.4	1034	500.5	90730
180	998.6	1090	531.7	100500
190	1036	1145	562.6	110700
200	1072	1199	593.0	121200
210	1109	1252	623.2	132100
220	1146	1305	653.0	143400
230	1207	1357	682.5	155100
240	1227	1409	711.6	167300
250	1253	1459	740.5	179700
260	1287	1509	769.1	192400
270	1325	1558	797.5	205400
280	1363	1607	825.5	218900
290	1401	1656	853.3	232700
298.15	1432	1695	875.8	244200
300	1440	1704	880.9	246900
310	1481	1752	908.2	261500
320	1526	1799	935.3	276500
330	1574	1847	962.2	292000
340	1625	1895	988.9	308000

$Li_2Co_2(Piv)_6$:

$$\mathrm{LnP}\ [Li_2Co_2(Piv)_6]\ (\mathrm{Pa}) = -(21121 \pm 866)/T + 41.1 \pm 0.6 (459 < T < 510\ \mathrm{K}).$$

The thermodynamic functions of compound **2** obtained from the adiabatic calorimetry data are given in Table 2.

The temperature dependence of C_p for complex **2** (Fig. 5) in the 210–250 K range shows two anomalies with the parameters $\triangle S^0 = 1.2$ and 0.3 J/(K mol) and $\triangle H^0 = 260$ and 80 J/mol. These anomalies are well reproduced, and their characteristics are independent of the thermal history of the sample. To elucidate the nature of anomalies, we measured the unit cell parameters of the complex at 298 and 198 K (Table S4). It appeared that the crystal system and the space group of compound **2** remain unchanged in the temperature range under consideration. Apparently, this anomaly is associated with the freezing of vibrations of the *tert*-butyl substituents at the carboxylate groups, Previously, we have observed an analogous effect for the heteronuclear complex $Co_2Sm(Piv)_7(2,4\text{-Lut})_2$ [40] and the coordination polymer $[Li_2Co_2(Piv)_6(\mu\text{-}L)_2]_n$, where L=2-amino-5-methylpyridine [16].

3.3. Preparation of $LiCoO_2$ films

To optimize the conditions for the synthesis of lithium cobaltate films from solution, the temperature program was

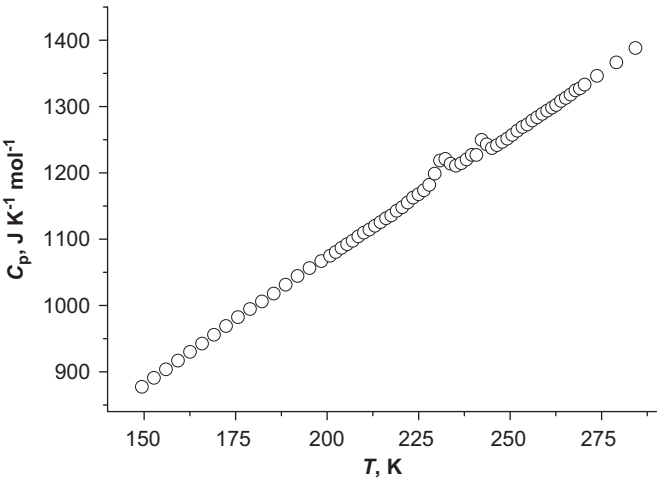

Fig. 5. Temperature dependence of the heat capacity of compound **2** in the 150–290 K range.

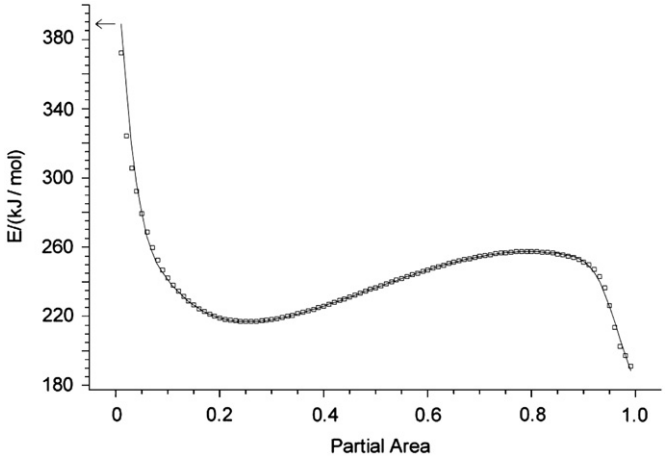

Fig. 6. Plot of the activation energy of the reaction $Li_2Co_2(Piv)_6(NEt_3)_{2(S)} \rightarrow Li_2Co_2(Piv)_6(NEt_3)_{(S)} + NEt_{3(G)}$ versus the degree of conversion.

calculated, and the thermolysis of **2** was performed at a controlled rate of gas evolution (3%/min). The program was devised based on the mathematical model for the first step of thermolysis of complex **2** obtained according to the above-described method. In the first step, the isoconversional analysis of the experimental data was carried out. The results were interpreted with the use of a procedure described in [33]. The dependence of the calculated activation energy (E_A) on the degree of conversion gives reliable evidence that the reaction involves more than one step. This situation was observed for complex **2** (Fig. 6).

In the beginning of the process (at $x < 0.2$), the activation energy sharply decreases, which is characteristic of the reactions involving the first reversible step $A \overset{I}{\leftrightarrow} B \xrightarrow{II} C$. In the range $x \sim 0.2$–0.7, the activation energy slowly increases from (217.0 ± 9.4) kJ/mol and reaches the maximum of (256.9 ± 15.1) kJ/mol at $x \sim 0.75$ followed by a plateau region ($x \sim 0.75$–0.8). This course of the curve is indicative of the presence of at least two events in this range. A sharp decrease in the activation energy at high degrees of conversion ($x > 0.9$) is typical of many thermolysis reactions [28]. The knowledge on the reaction mechanism is summarized in the scheme.

$$A \overset{I}{\underset{Cn,An}{\leftrightarrow}} B \begin{array}{l} \xrightarrow[E \le 226.4\ \mathrm{kJ/mol}]{II} C \\ \xrightarrow[E \sim 256.9\ \mathrm{kJ/mol}]{III} D \end{array} \xrightarrow[E \le 226.1\ \mathrm{kJ/mol}]{IV\ diff} E \qquad (5)$$

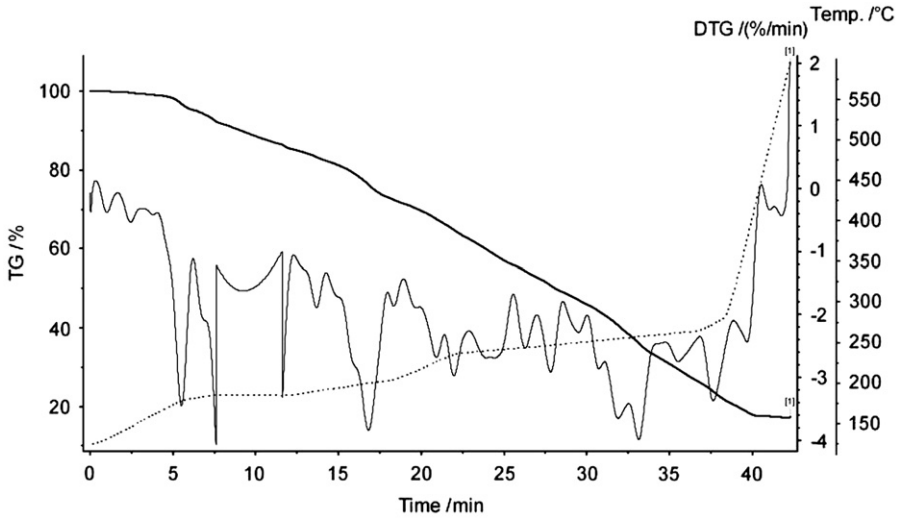

Fig. 7. TGA results for the thermolysis of the complex $Li_2Co_2(Piv)_6(NEt_3)_2$ obtained with the use of the calculated temperature program (%): the TG signal, the DTG signal, and the temperature are indicated by a thick line, a thin line, and a dashed line, respectively.

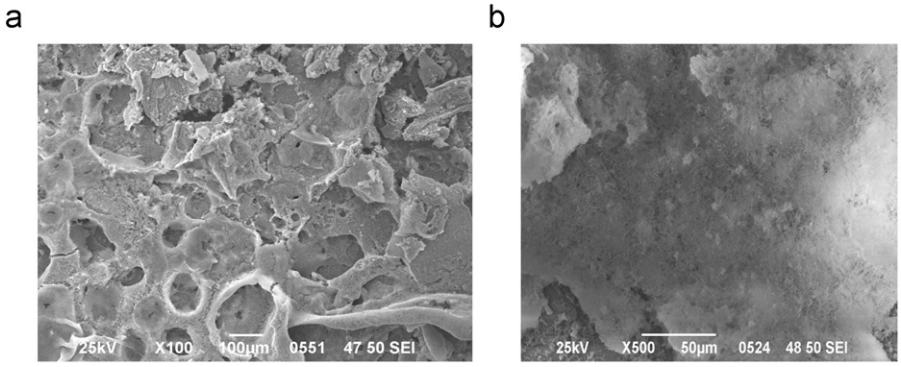

Fig. 8. Photomicrographs of $LiCoO_2$ films; a sapphire substrate; the calcination temperature was 500 °C ((a) the heating rate was 10 deg./min; (b) the temperature program).

In the next step, the parameters of the preliminary scheme of the process and its variations were optimized by nonlinear regression using different types of the function $f(x)$. The parameters of the reaction steps calculated according to the Ozawa–Flynn–Wall method and the nonlinear regression are in satisfactory agreement. The consistency of the results of the non-*a-priori* and model-fitting analysis and the agreement between the results of the simulation based on the data obtained by different methods (TGA and DSC) confirm the validity of the above-described model. The results of the simulation of the thermolysis mechanism were used for the calculation of the temperature program, which made it possible to maintain the rate of gas evolution at a specified level during the decomposition of the complex to $LiCoO_2$ (Fig. 7). The experimental curves are consistent with the limitations on the rate of gas evolution (3%/min) determined in the calculations of the temperature program.

The films prepared by the decomposition of the complex in solution with the use of this program were relatively uniform (Fig. 8).

4. Conclusions

A new heterometallic complex $Li_2Co_2(Piv)_6(NEt_3)_2$ (**2**) with a good leaving neutral NEt_3 ligand was synthesized in high yield (95%). The molecular and crystal structure of **2** was established. The magnetic behavior of complex **2** was investigated and the thermodynamic characteristics were obtained. Thermal transformations in the crystals of complex **2** without a change in the crystal system and the space group were observed before the onset of thermal decomposition in the 210–250 K temperature range. These transformations are apparently attributed to a change in intramolecular motion. Based on the data on the vaporization process and solid-state thermolysis, complex **2** can be recommended as a potential molecular precursor for the synthesis of thin films of lithium cobaltate $LiCoO_2$.

5. Supplementary data

The supplementary file contains Tables S1–S4 with legends. CCDC 749978 contains the supplementary crystallographic data for compound **2**. These data can be obtained free of charge via http://www.ccdc.cam.ac.uk/conts/retrieving.html, or from the Cambridge Crystallographic Data Centre, 12 Union Road, Cambridge CB2 1EZ, UK; fax: (+44) 1223-336-033; or e-mail: deposit@ccdc.cam.ac.uk.

Acknowledgments

This study was supported by the Russian Foundation for Basic Research (project nos. 08-03-00091, 08-03-00365, 09-03-90441,

09-03-12228, 09-03-12122, and 08-03-00343), the Council on Grants of the President of the Russian Federation (grants NSh-3672.2010.3, NSh-8503.2010.3, MK-156.2009.3), the State Department of Science and Innovation Policy (NK-537P_25), the Russian Science Support Foundation, the Russian Academy of Science, the Siberian Branch of the Russian Academy of Sciences and the Department of Chemistry and Materials Science. Partially the work is performed at User Facilities Center of M.V. Lomonosov Moscow State University.

Appendix A. Supplementary materials

Supplementary data associated with this article can be found in the online version at doi:10.1016/j.jssc.2010.08.007

References

[1] R.W. Schwartz, Chem. Mater. 9 (1997) 2325.
[2] K.A. Vorotilov, M.I. Yanovskaya, E.P. Turevskaya, J. Sol–Gel Sci. Technol. 16 (1999) 109.
[3] A.R. Kaul, O.Yu. Gorbenko, A.A. Kamenev, Russ. Chem. Rev. Int. Ed. 73 (2004) 861.
[4] V.N. Vertoprakhov, L.D. Nikulina, I.K. Igumenov, Russ. Chem. Rev. Int. Ed. 74 (2005) 797.
[5] M.S. Bhuiyan, M. Paranthaman, K. Salama, Supercond. Sci. Technol. 19 (2006) R1.
[6] D. Caruntu, Y. Remond, N.H. Chou, M.-J. Jun, G. Caruntu, J. He, G. Goloverda, C. O'Connor, V. Kolesnichenko, Inorg. Chem. 41 (2002) 6137.
[7] M. Stefanescu, O. Stefanescu, M. Stoia, C. Lazau, J. Therm., Anal. Cal. 88 (2007) 27.
[8] R. Frycek, F. Vyslouzil, V. Myslik, M. Vrnata, D. Kopecky, O. Ekrt, P. Fitl, M. Jeli´nek, T. Kocourek, R. Sipula, Sensors Actuators 125 (2007) 189B 125 (2007) 189.
[9] H. Thakuria, B.M. Borah, G. Das, Eur. J. Inorg. Chem. (2007) 524.
[10] O. Carp, L. Patron, I. Mindru, G. Marinescu, L. Diamandescu, A. Banuta, J. Therm. Anal. Calorim. 74 (2003) 789.
[11] A.V. Rudchenko, Yu.K. Pirinskii, O.V. Nesterova, V.N. Kokozay, Ukr. Khim. Zh. 9/10 (2004) 61.
[12] Yu.K. Pirinskii, V.S. Kublanovskii, A.V. Berezovskaya, A.A. Beznischenko, V.N. Kokozay, V.G. Makhankoya, Rep. Natl. Acad. Sci. Ukraine 6 (2008) 133.
[13] M. Hamid, A.A. Tahir, M. Mazhar, M. Zeller, K.C. Molloy, A.D. Hunter, Inorg. Chem. 45 (2006) 10457.
[14] N. Deb, S.D. Baruah, N.N. Dass, J. Therm. Anal. Cal. 59 (2000) 791.
[15] S.L. Tey, M.V. Reddy, G.V.S. Rao, B.V.R. Chowdari, J.J. Ding, J.J. Vittal, Chem. Mater. 18 (2006) 1587.
[16] M. Bykov, A. Emelina, M. Kiskin, A. Sidorov, G. Aleksandrov, A. Bogomyakov, Z. Dobrokhotova, V. Novotortsev, I. Eremenko, Polyhedron 28 (2009) 3628.
[17] D.V. Sevast'yanov, V.G. Sevast'yanov, E.P. Simonenko, Thermochim. Acta 381 (2002) 173.
[18] M.A. Golubnichaya, A.A. Sidorov, I.G. Fomina, M.O. Ponina, S.M. Deomidov, S.E. Nefedov, I.L. Eremenko, I.I. Moiseev, Russ. Chem. Bull. (Engl. Transl.) 48 (1999) 1751.
[19] SMART (Control) and SAINT (Integration) Software, Version 5.0, Bruker AXS Inc., Madison, WI,1997.
[20] G.M. Sheldrick, Acta Crystallogr. A 46 (1990) 467.
[21] G.M. Sheldrick, in: SHELXL-93, Program for the Refinement of Crystal Structures, University of Göttingen, Germany, 1993.
[22] R.M. Varushchenko, A.I. Druzhinina, E.L. Sorkin, J. Chem. Thermodyn. 29 (1997) 623.
[23] K.S. Gavrichev, N.N. Smirnova, V.M. Gurevich, V.P. Danilov, A.V. Tyurin, Ryumin, L.N. Komissarova, Thermochim. Acta 448 (2006) 63.
[24] V.M. Gurevich, O.L. Kuskov, K.S. Gavrichev, A.V. Tyurin, Geochem. Int. 45 (2007) 206.
[25] S.W. Kieffer, Rev. Geophys. Space Phys. 17 (1979) 35.
[26] V.M. Gurevich, V.E. Gorbunov, K.S. Gavrichev, I.L. Khodakovskii, Geochem. Int. 37 (1999) 367.
[27] M.E. Brown (Ed.), Introduction to Thermal Analysis. Techniques and Applications, second ed., Kluwer Academic Publishers, Dordrecht, 2004.
[28] G.W.H. Hohne, W.F. Hemminger, H.J. Flammersheim, in: Differential Scanning Calorimetry, second revised and enlarged ed., Springer, Berlin, 2003.
[29] H.L. Friedman, J. Polym. Lett. 4 (1966) 323.
[30] T. Ozawa, Bull. Chem. Soc. Japan 38 (1965) 1881.
[31] J. Flynn, L.A. Wall, J. Polym. Lett. 4 (1966) 232.
[32] J. Opfermann, J. Therm., Anal. Cal. 60 (2000) 641.
[33] S.V. Vyazovkin, C.A. Wight, Thermochim. Acta 340–341 (1999) 53.
[34] S.V. Vyazovkin, Thermochim. Acta 355 (2000) 155.
[35] A. Burnham, Thermochim. Acta 355 (2000) 165.
[36] H.J. Flammersheim, J.R. Opfermann, Thermochim. Acta 388 (2002) 389.
[37] Yu.V. Rakitin V.T., Kalinnikov, Sovremennaya magnetokhimiya, Nauka. St-Petersburg, 1994 (in Russian) [Modern magnetochemistry, Science. St. Petersburg, 1994].
[38] J.B. Mann, J. Chem. Phys. 46 (1967) 1646.
[39] I.W. Otvos, D.P. Stevenson, J. Chem. Soc. 78 (1956) 546.
[40] M.A. Bykov, A.L. Emelina, M.A. Kiskin, G.G. Aleksandrov, A.S. Bogomyakov, Zh.V. Dobrokhotova, V.M. Novotortsev, I.L. Eremenko, Russ. J. Inorg. Chem. Int. Ed. 54 (2009) 548.